

Upscaling Flux Observations from Local to Continental Scales Using Thermal Remote Sensing

Martha C. Anderson,* William P. Kustas, and John M. Norman

ABSTRACT

A number of recent intensive and extended field campaigns have been devoted to the collection of land-surface fluxes from a variety of platforms, with the purpose of inferring the long-term C, water, and energy budgets across large areas (watershed, continental, or global scales). One approach to flux upscaling is to use land-atmosphere transfer schemes (LATS) linked to remotely sensed boundary conditions as an intermediary between the sensor footprint and regional scales. In this capacity, we examined the utility of a multiscale LATS framework that uses thermal, visible and near infrared remote sensing imagery from multiple satellites to partition surface temperature and fluxes between the soil and canopy. We conducted exercises using tower and aircraft flux data collected at three experiment sites in Oklahoma and Iowa, each with a different configuration of instrumentation. Combined, the two flux-monitoring systems were found to be complementary: the towers provided high-spatial-resolution, time-continuous validation at discrete points within the modeling domain, while with the aircraft data it could be confirmed that the model was reproducing broad spatial patterns observed at specific moments in time. High-resolution flux maps created with the LATS allowed evaluation of differences in footprint associated with turbulent, radiative, and conductive flux sensors, which may be contributing to energy budget closure problems observed with eddy correlation systems. The ability to map fluxes at multiple resolutions (1 m–10 km) with a common model framework is beneficial in providing spatial context to an experiment by bracketing the scale of interest. Multiscale flux maps can also assist in the experimental design stage, in *a priori* assessments of sensor representativeness in complex landscapes.

DURING THE LAST TWO DECADES, several intensive field campaigns have focused on collecting high-quality surface flux measurements from tower and aircraft platforms deployed over a wide variety of landscapes and under many different climatic conditions (e.g., FIFE [Kanemasu et al., 1992], Monsoon '90 [Stannard et al., 1994], HAPEX-SAHEL [Goutorbe et al., 1994], BOREAS [Sellers et al., 1997], and the Soil Moisture–Atmospheric Coupling Experiment [SMACEX; Prueger et al., 2005]). In addition, routine, interannual flux measurements are being made at an increasing number of locations to facilitate large-scale environmental monitoring. Running et al. (1999), for example, described a global network for monitoring terrestrial C fluxes using tower-based measurements and airborne flask sampling. The flux data

sets collected in these experiments will ultimately be upscaled to make inferences regarding the long-term C, water, and energy budgets across large areas (watershed, continental, or global scales).

To this end, an upscaling mechanism must be used to fill temporal and spatial gaps that remain unsampled by the deployed flux instrumentation set. Eddy correlation (EC) systems integrate fluxes arising from a “source area” or “footprint” on the land surface only of order 10^2 to 10^3 m in dimension, depending on sensor height above ground level (agl). Spatial coverage has been improved in many experiments by flying EC systems on aircraft, often on transects intersecting ground-based tower locations for intercomparison (Desjardins et al., 1997; Samuelson and Tjernström, 1999; Stephens et al., 2000; Mahrt et al., 2001; Song and Wesely, 2003; Prueger et al., 2005). A major challenge for such experiments is to ensure that the combined flux data sets are adequately characterizing the full heterogeneity present in the landscape (Schmid, 1997; Schmid and Lloyd, 1999), and to find reasonable means for comparing data from tower and aircraft sensors, which generally are sampling very different footprints on the land surface (Kaharabata et al., 1997). Furthermore, a reliable procedure must be identified for extrapolating these findings to times and locations outside of the field study domain.

One approach to flux upscaling uses LATS linked to remotely sensed boundary conditions as an intermediary between the sensor footprint and regional scales. Modeled flux fields provide a basis for connecting point-like tower data and linear aircraft transect measurements made at height with the two-dimensional patterns of fluxes diagnosed at the land surface. The tower and aircraft fluxes can be backprojected onto the surface source and sink distribution through inversion of an appropriate advection–dispersion model, defining the effective “source weighting function” (see review by Schmid, 2002). If the comparisons are reasonable within the segment of the experimental domain sampled by the measurement sets, gridded model fluxes can be aggregated with some degree of confidence to larger spatiotemporal scales with similar characteristics.

M.C. Anderson and W.P. Kustas, USDA-ARS, Hydrology and Remote Sensing Lab., Bldg. 007, BARC West, 10300 Baltimore Ave., Beltsville, MD 20705; and J.M. Norman, Dep. of Soil Science, Univ. of Wisconsin, Madison, WI 53706. Received 1 Apr. 2005. *Corresponding author (manderson@hydrolab.arsusda.gov).

Published in *Agron. J.* 99:240–254 (2007).

Special Submissions

doi:10.2134/agronj2005.0096S

© American Society of Agronomy

677 S. Segoe Rd., Madison, WI 53711 USA

Abbreviations: ABL, atmospheric boundary layer; agl, above ground level; ALEXI, Atmosphere–Land Exchange Inverse; ASTER, Advanced Space-borne Thermal Emission Reflectance Radiometer; EC, eddy correlation; ER, El Reno, OK; ET, evapotranspiration; GOES, Geostationary Operational Environmental Satellite; LAI, leaf area index; Landsat, Land Remote-Sensing Satellite; LATS, land-atmosphere transfer scheme; OASIS, Oklahoma Atmospheric Surface-Layer Instrumentation System; RMSD, root mean square difference; SMACEX, Soil Moisture–Atmospheric Coupling Experiment; SPG97, Southern Great Plains Experiment of 1997; TIMS, Thermal Infrared Multispectral Scanner; TSEB, two-source surface energy balance; vis/NIR, visible and near infrared.

While a diverse set of measurements is required for model validation under this type of aggregation strategy, characterizing the range in biotic and climatic conditions expected within the target region, the exact statistical representativeness of the measurement sites is less important. The remote sensing data guide the weighting of flux variability in the upscaling process by tying the model flux fields directly to observed spatial structure in land-surface conditions that is relevant to flux partitioning. The discussion here focuses on a multiscale LATS framework that uses thermal and visible and near infrared (vis/NIR) remote sensing imagery to approximate surface temperature and vegetation cover distributions across a study area. Combined, these remotely sensed input fields provide information about surface moisture status and coupling between the surface and atmosphere—factors that strongly influence water, energy, and C fluxes.

Upscaling exercises have been conducted using tower and aircraft flux data collected at three experiment sites in Oklahoma and Iowa. Based on these experiments, the effect of tower network density and configuration on comparisons with regional-scale models has been evaluated, along with the value added by including aircraft-based flux measurements in the validation effort. We also examined the source area footprints associated with various flux measurements, and how differences in footprint may contribute to errors in the observed energy budget closure. Multiscale LATS modeling can also be used in the experimental design stage to determine optimal deployment of instrumentation for assessing large-scale flux conditions.

MODEL DESCRIPTION

An effective flux-upscaling scheme must bridge the gap between the tower footprint scale (~100 m) and the target scale of interest (thousands of kilometers for the continental USA). Here we examine an economical approach to upscaling, using a targeted flux disaggregation strategy. Fluxes are mapped across regional or continental scales at 5- to 10-km resolution each day using coarse-scale remote sensing imagery from a geostationary platform like the Geostationary Operational Environmental Satellite (GOES). These coarse-scale flux estimates can then be spatially disaggregated to finer scales at sites of particular interest (e.g., around a flux tower, an aircraft flight line, or a field experiment site) using higher resolution imagery from the Land Remote-Sensing Satellite (Landsat), the Advanced Space-borne Thermal Emission Reflectance Radiometer (ASTER), or the Moderate Resolution Imaging Spectroradiometer (MODIS) whenever such imagery is available (as determined by the satellite overpass schedule and cloud conditions). In this way, the temporal sampling power of the geostationary satellites (images every 15 min) can be combined with the spatial resolution of polar orbiters (15 m–1 km). The disaggregation process serves both as a means for quantitatively validating the regional flux predictions and for examining complex landscapes of interest in greater detail, as will be seen below.

Two-Source Energy Balance Model (Local Scale)

The LATS modeling system we used was built around the two-source energy balance (TSEB) approach of Norman et al. (1995; see also Kustas and Norman, 1999, 2000), which partitions the composite surface radiometric temperature, T_{RAD} , into apparent soil and canopy temperatures, T_S and T_C , based on the local vegetation cover fraction apparent at the thermal sensor view angle, $f(\theta)$:

$$T_{\text{RAD}}(\theta) = \{f(\theta)T_C^4 + [1 - f(\theta)]T_S^4\}^{1/4} \quad [1]$$

(Fig. 1a). With this information, the TSEB evaluates the soil (subscript S) and the canopy (subscript C) energy budgets separately, computing system and component fluxes of net radiation ($RN = RN_C + RN_S$), sensible and latent heat ($H = H_C + H_S$ and $\lambda E = \lambda E_C + \lambda E_S$), and ground heat conduction (G):

$$\begin{aligned} RN &= H + \lambda E + G \\ RN_S &= H_S + \lambda E_S + G \\ RN_C &= H_C + \lambda E_C \end{aligned} \quad [2]$$

Canopy and soil sensible heat fluxes are evaluated from temperature gradients across the series resistance network in Fig. 1 with endpoints T_S , T_C , and T_A , where T_A is an estimate of air temperature above the canopy. Extinction of net radiation within the canopy (RN_C) is approximated with an analytical formalism described by Campbell and Norman (1998) based primarily on leaf absorptivity and leaf area index (LAI), while G is parameterized as a fraction (0.31) of the net radiation above the soil surface (RN_S), following Choudhury et al. (1994). A modified Priestley–Taylor relationship (Priestley and Taylor, 1972) provides an initial estimate of canopy evapotranspiration (λE_C ; Tanner and Jury, 1976), which is reduced if signs of vegetation stress are detected in the thermal land-surface signature. Finally, the soil evaporation rate (λE_S) is computed as a residual to the system energy budget.

This two-source surface representation has been found to have several important advantages in comparison with single-source thermal models, which do not distinguish between soil and canopy contributions (Zhan et al., 1996; Kustas et al., 2004). First, the TSEB treats surface transfer coefficients more realistically. While soil and vegetation components contribute to the radiative temperature of the scene roughly in proportion to their fractional coverage (Eq. [1]), they contribute to the system sensible heat flux in proportion to their atmospheric coupling, as reflected in the diffusive soil and foliage boundary layer resistances, R_S and R_X , respectively, in Fig. 1. One-source models lump the effects of R_S and R_X into the form of a bulk empirical “excess resistance” or “ kB^{-1} ” term, which is difficult to parameterize accurately, particularly for scenes with sparse vegetation (e.g., Kustas et al., 1989; Stewart et al., 1994; Verhoef et al., 1997). With the TSEB, a single model formulation can be applied to a wide range in surface conditions: from bare soil to partial vegetation to full cover. The additional input required over single-source models is the vegetation cover fraction, a quantity available from remote sensing.

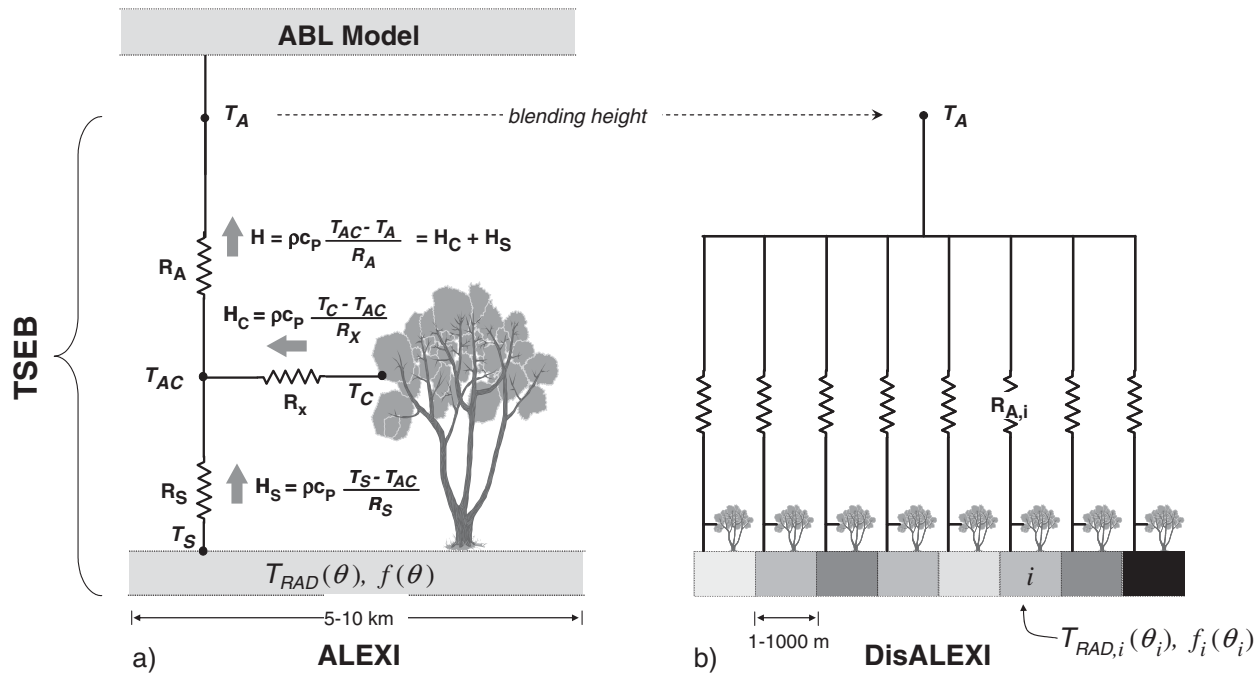


Fig. 1. Schematic diagram representing the (a) ALEXI and (b) DisALEXI modeling schemes, coupling atmospheric boundary layer (ABL) and two-source surface energy balance (TSEB) submodels. The models compute fluxes of sensible heat (H) from the soil and canopy (subscripts c and s) along gradients in temperature (T), and regulated by transport resistances R_A (aerodynamic), R_x (bulk leaf boundary layer) and R_S (soil surface boundary layer). DisALEXI uses the air temperature predicted by ALEXI near the blending height (T_A) to disaggregate 5-km ALEXI fluxes, given vegetation cover [$f(\theta_i)$] and directional surface radiometric temperature [$T_{RAD}(\theta_i)$] information derived from high-resolution remote-sensing imagery at look angles θ_i . See Norman et al. (2003) for further details.

Another important feature of the two-source model, from an operational standpoint, is that it can accommodate thermal data acquired at off-nadir viewing angles such as from an aircraft or satellite platform. From geometrical considerations, the fraction of view occupied by bare soil (relatively hot) is maximized at a nadir view angle and minimized at oblique angles due to obscuration by vegetation (relatively cool). The exact angular shape of this function [and $f(\theta)$] will depend on canopy architecture, primarily the degree to which foliar elements are clumped, both at the plant scale and at row or plot scales (Kucharik et al., 1999; Anderson et al., 2005). The expected variation in composite T_{RAD} can be modeled knowing the soil and canopy temperatures (provided by the TSEB) and the angular dependence of the canopy gap fraction, $[1 - f(\theta)]$, as described by Beer's Law. While one-source model evaluations are typically restricted to a narrow range in acceptable sensor view angle (Vining and Blad, 1992), the TSEB has been shown to be effective using data both from GOES at look angles of $\sim 50^\circ$ from nadir and from Landsat at $\sim 5^\circ$ (Anderson et al., 2004, 2005) for a wide range of canopy characteristics. The utility of these methods for view angles $> 50^\circ$ has yet to be evaluated.

ALEXI (Regional Scale)

A major challenge in thermal-based flux modeling lies in specifying the required meteorological boundary conditions in air temperature, T_A , with adequate accuracy. In regional-scale analyses of surface fluxes, this input field is often interpolated from standard synoptic mea-

surements, with typical spacing in the USA of 100 km. Feedback between the surface and atmosphere, however, can cause local conditions to be very different from shelter-level conditions at the nearest synoptic station. Given that standard meteorological data are typically collected at airports over grass, interpolation of T_A to intermediate pixels with disparate land-surface conditions can cause large errors in the assumed vertical temperature gradient used to compute H (Fig. 1).

The need for near-surface meteorological inputs can be alleviated by coupling the surface model with an atmospheric boundary layer (ABL) model, thereby simulating land-atmosphere feedback internally (Carlson, 1986). In the Atmosphere-Land Exchange Inverse (ALEXI) model (Anderson et al., 1997), the TSEB is applied at two times during the morning boundary layer growth phase (~ 1.5 and 5.5 h after sunrise), using radiometric temperature data obtained from a geostationary platform like GOES. Energy closure over this interval is provided by a simple slab model of ABL development (McNaughton and Spriggs, 1986), relating the rise in air temperature in the mixed layer to the time-integrated influx of sensible heat from the land surface. Given a diagnosis of air temperature at the interface between the surface and ABL model components, the vertical temperature gradient and sensible heat flux in the surface layer can be estimated. This coupling effectively moves the upper boundary conditions in temperature from shelter level to higher up in the atmosphere where conditions are more uniform at the model grid scale of 5 to 10 km. Because ALEXI is built around a time-differential radiometric signal (the morning surface temperature rise)

rather than an absolute temperature, it is less sensitive to errors in atmospheric corrections, sensor calibration, and surface emissivity specification because the time-independent component of these corrections is eliminated (Kustas et al., 2001). Furthermore, due to its time-differential nature, ALEXI uses only the general slope (lapse rate) of the atmospheric temperature profile (Anderson et al., 1997), which is more reliably analyzed from operational radiosonde network data than is the absolute temperature reference.

DisALEXI (Flux Disaggregation)

Given its coupled nature, ALEXI is constrained to work at fairly coarse spatial scales of 5 to 10 km or greater, where mean land-surface conditions become effective in influencing the ABL (Avissar and Schmidt, 1998). Across heterogeneous landscapes, the TSEB can also be used to model fluxes at finer scales using a “tile” or “mosaic” approach (Koster and Suarez, 1992), provided that the upper boundary meteorological inputs are supplied at sufficient height such that subgrid-scale effects have become well blended and conditions are relatively uniform across the modeling area (see Fig. 1b). The problem is that the “blending height” (on the order of 10^2 m; Wieringa, 1976, 1986; Mason, 1988) temperature is not generally known locally, except in specialized field experiments from radiosonde or aircraft measurements. Even if such measurements were routinely available, there is no guarantee of good calibration between the air and thermal land-surface temperature sensors, which operate under very different physical principles.

For routine applications, the regional ALEXI model can be used to simulate a mixed-layer temperature above the blending height, at the interface between the TSEB and ABL submodels. This modeled air temperature is, in some cases, preferable to actual measurements made aloft because it can adjust to some extent to instrumental biases in the thermal remote sensing data (Anderson et al., 1997). A tile application of the TSEB using T_A derived by ALEXI effectively constitutes a spatial disaggregation of the ALEXI sensible heat flux estimate, and therefore this process is referred to as DisALEXI (Norman et al., 2003; Fig. 1).

FLUX DATA SETS

To date, the ALEXI–DisALEXI modeling system has been applied at three experiment sites, each with a different configuration of flux measurement instrumentation (see Table 1). Comparison of these validation exercises allows an analysis of optimal experimental design. In each case, the ALEXI model was used to create 5-km resolution flux maps of the study area with temperature data from the GOES imager and vegetation cover fraction from the Advanced Very High Resolution Radiometer. Downwelling long- and short-wave components of net radiation were extracted from 20-km GOES-based estimates (Diak et al., 2000; Otkin et al., 2005), while ancillary gridded meteorological data (including wind speed and atmospheric temperature profile) have been obtained from mesoscale analyses of

Table 1. Summary of model and tower flux data sets.

Experiment	ALEXI dates	DisALEXI dates	Towers† no.	Tower density
OASIS (Oklahoma)	29 May 2000	29 May 2000	7	1 per ALEXI grid cell
	12 Aug. 2000	12 Aug. 2000		
	10 June 2001	10 June 2001		
	12 July 2001	12 July 2001		
SGP97 (Oklahoma)	29 June 1997	29 June 1997	4	4 per ALEXI grid cell
	1 July 1997	1 July 1997		
	2 July 1997	2 July 1997		
SMACEX (Iowa)	16 June 2002	23 June 2002	12	12 per 8 ALEXI grid cell
	23 June 2002			
	27 June 2002			
	28 June 2002			
	1 July 2002	1 July 2002		
	2 July 2002			

† Instrumental issues resulted in occasional data loss from a subset of these towers on some modeling dates.

standard synoptic data sets. The ALEXI grid cells containing measurement sites were disaggregated to 24 to 90 m using high-resolution thermal and vis/NIR imagery from Landsat, ASTER, or an airborne imaging system.

Oklahoma Atmospheric Surface-Layer Instrumentation System

The Oklahoma Atmospheric Surface-Layer Instrumentation System (OASIS; Brotzge et al., 1999) consists of 10 towers equipped with EC systems sited in different climatic zones across the state. The system went online in 1999 and has operated continuously ever since. The flux and radiation instrumentation at these OASIS “super sites” have been described by Brotzge and Weber (2002) and Basara and Crawford (2002); these include EC equipment mounted on a tower at 4.5 m agl, a net radiation sensor at 2 m agl, and a soil heat flux system near the tower base. The typical spacing between super sites is ~200 km, so the OASIS network provides no more than one EC tower per 5-km ALEXI grid cell. Combined, the towers sample several land-use and land-cover types, including pasture, scrub, and agricultural lands.

In the experiment described by Anderson et al. (2004), 5-km ALEXI fluxes were disaggregated to 30-m resolution at seven OASIS super sites using thermal and vis/NIR imagery from Landsat 7 (see Fig. 2). Four clear Landsat scenes were selected from May through August in 2000 and 2001, representing varying climatic conditions; the Norman, OK, super site (NORM) was included in scenes on two different dates. The thermal imagery used in the disaggregation was sharpened from its native resolution of 60 m to the 30-m resolution of the Enhanced Thematic Mapper vis/NIR bands using a technique described by Kustas et al. (2003), which exploits the covariation between temperature and vegetation index observed within a given scene.

Southern Great Plains Experiment of 1997

The Southern Great Plains Experiment of 1997 (SGP97; Jackson et al., 1999) hosted a high-density network of EC towers in the USDA-ARS Grazinglands Research Facility near El Reno, OK. In the experiment reported by Nor-

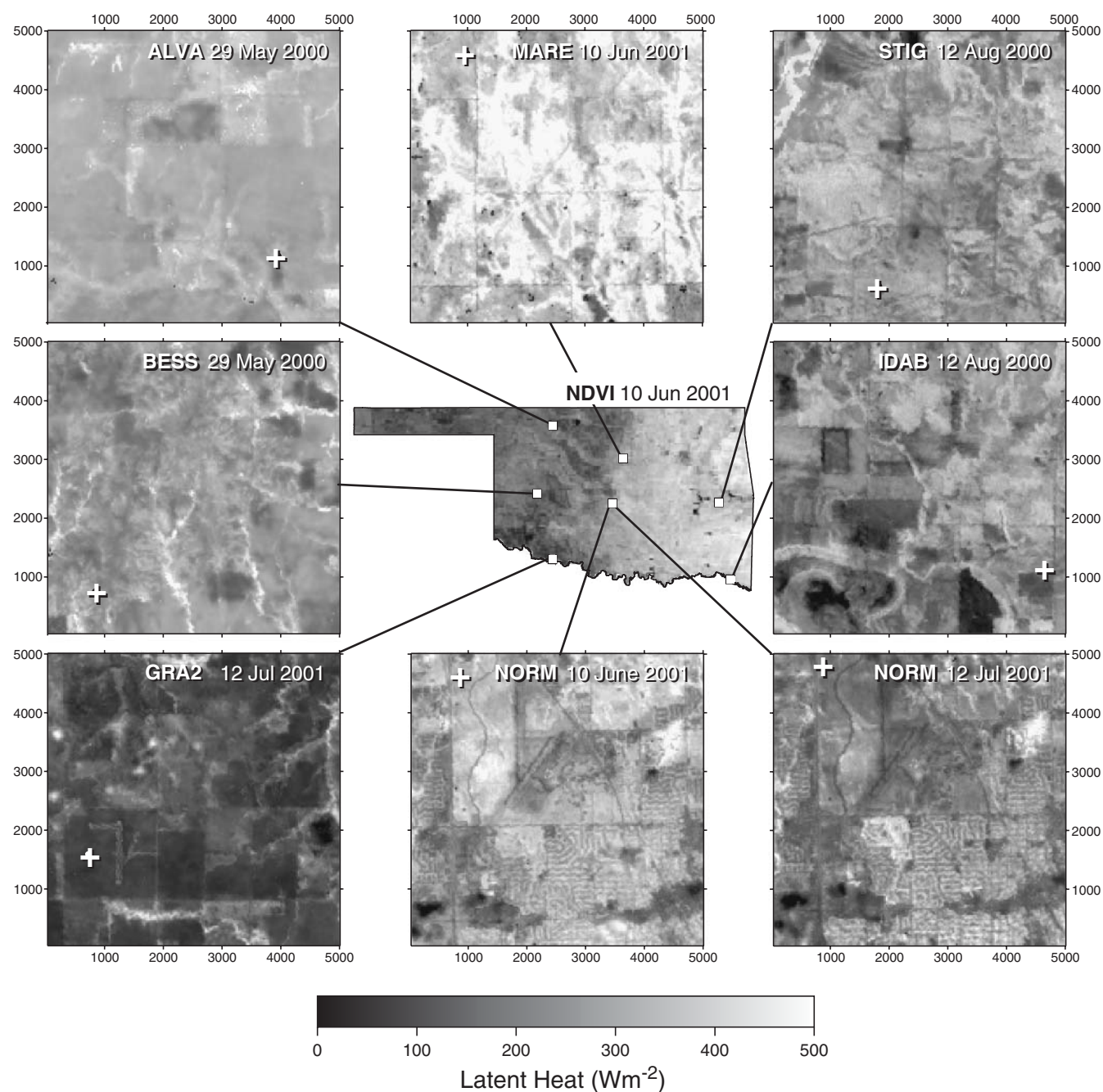


Fig. 2. Disaggregated maps of latent heating (30-m resolution) in 5-km ALEXI grid cells around eddy-correlation (EC) towers in the OASIS network. Crosses indicate the location of the towers, with no more than one tower per grid cell. Axes are labeled as distance in meters.

man et al. (2003), data from four EC towers in one 5-km ALEXI grid cell were used for model validation: three were in pastures with LAI varying from 2.6 to 4.7, and one was in a bare field of recently harvested winter wheat (*Triticum aestivum* L.; Fig. 3). The EC and net radiation sensors were mounted at approximately 2 m agl.

Norman et al. (2003) focused on a 4-d dry-down period following a major rainfall event on 28 June 1997, where patchy areas of latent heating developed due to variations in vegetation cover. Evaporation from tilled fields and wheat stubble was cut off rapidly as the soil surface dried, in comparison with pasture and riparian

areas, which maintained potential evapotranspiration (ET) throughout the dry-down. This led to well-defined localized areas of high sensible heating superposed on a moister background.

In addition to the flux tower network, EC and net radiation instrumentation was also flown over the El Reno (ER) study area on a Twin Otter aircraft operated by the National Research Council (NRC) of Canada (MacPherson, 1998) along a transect of ~15 km in length and at a height of ~35 m agl (also shown in Fig. 3). From data collected across the full ER transects, Mahrt et al. (2001) computed segmented flux values over 1-km

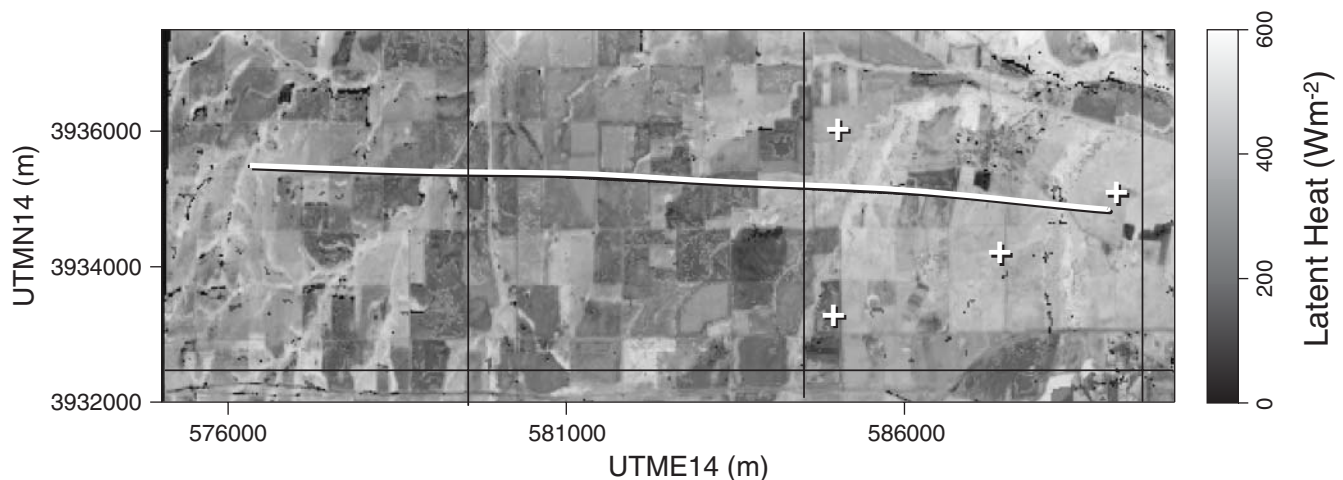


Fig. 3. Disaggregated latent heating estimates (24-m resolution) on 2 July 1997 over the El Reno study area during SGP97, projected to UTM Zone 14 coordinates. Crosses indicate locations of four flux towers, while the white line shows the El Reno (ER) track flown by the Canadian Twin Otter aircraft. Black lines represent the scale of the 5-km ALEXI grid. In this case, all towers were located in the same ALEXI grid cell.

intervals, which they then subsampled using a 250-m moving window with a new scheme for estimating the time–space dependence of surface fluxes.

Disaggregation of ALEXI fluxes over the tower and aircraft transect sites was accomplished using high-resolution imagery collected by airborne sensors on 3 d during the dry-down: thermal maps were created with the Thermal Infrared Multispectral Scanner (TIMS; Palluconi and Meeks, 1985), while LAI was derived from maps of the normalized difference vegetation index created with the Thematic Mapper Simulator. Both temperature and LAI maps were aggregated from 12- to 24-m resolution to reduce registration errors (see Norman et al., 2003, for further details).

Soil Moisture–Atmospheric Coupling Experiment

The Soil Moisture–Atmospheric Coupling Experiment (SMACEX; Kustas et al., 2005) was part of the 2002 soil moisture experiment conducted in the Walnut Creek Watershed just south of Ames, IA. The purpose of SMACEX was to study the upscaled effects of field-scale heterogeneity in vegetation and soil moisture conditions on regional surface fluxes and boundary layer development. To this end, 12 EC towers were deployed in corn (*Zea mays* L.) and soybean [*Glycine max* (L.) Merr.] fields across a 10- by 20-km area around Walnut Creek (see Fig. 4). The EC instruments were maintained at levels at least twice the height of the canopy, ranging from 2 to 5 m agl (see Prueger et al., 2005).

On several days during SMACEX, the NRC Twin Otter aircraft flew several missions over the Walnut Creek study area on transects designed to intersect many of the EC towers. Turbulent fluxes of heat, water, CO₂, ozone, and momentum were measured at an altitude of ~40 m on repeated passes over six tracks ranging in length from 6 to 12 km (Fig. 4). Net radiation was also measured from the aircraft at nadir view. Details of the aircraft-based measurements are given by MacPherson and Wolde (2002) and MacPherson et al. (2003).

As described by Anderson et al. (2005), ALEXI fluxes over the Walnut Creek study area were disaggregated to the 60- to 120-m scale using thermal and vis/NIR imagery on 2 d acquired by Landsat 5 and Landsat 7. The same scene has been disaggregated to 90 m using ASTER imagery for a comparison study of thermal-based flux models (French et al., 2005).

Closure Corrections

Comparisons between EC flux measurements and model predictions are often complicated by a lack of “closure” in the observed energy budget. Typically, $RN - G > H + \lambda E$ in EC data sets (Desjardins et al., 1997; Mahrt, 1998; Twine et al., 2000; Wilson et al., 2002), while surface energy balance models by definition enforce closure among flux estimates. At the present time, the source of this systematic discrepancy is not clearly understood—whether the measured turbulent fluxes of H and λE are in error, or if some other component of the energy budget is not being accounted for. To demonstrate the magnitude of this uncertainty, we quote tower and aircraft H and λE fluxes both as measured (unclosed), and with an energy budget closure correction (closed) preserving the observed Bowen ratio (Twine et al., 2000). Alternately, some have suggested that for high evaporative fluxes the entire residual ($RN - G - H - \lambda E$) should be attributed to λE (Brotzge and Crawford, 2003; Prueger et al., 2005). In such cases, however, the Bowen ratio is low and the method of Twine et al. (2000) apportionments most of the residual to λE anyway. The average G measured at the EC tower sites within each study area has been used to close the aircraft budgets.

MODEL COMPARISONS WITH TOWER FLUXES

Examples of disaggregated latent heat flux maps from each experiment are shown in Fig. 2 to 4. These model simulations suggest that an instantaneous tower-based flux measurement could vary by several hundred watts per square meter depending on exactly where the tower

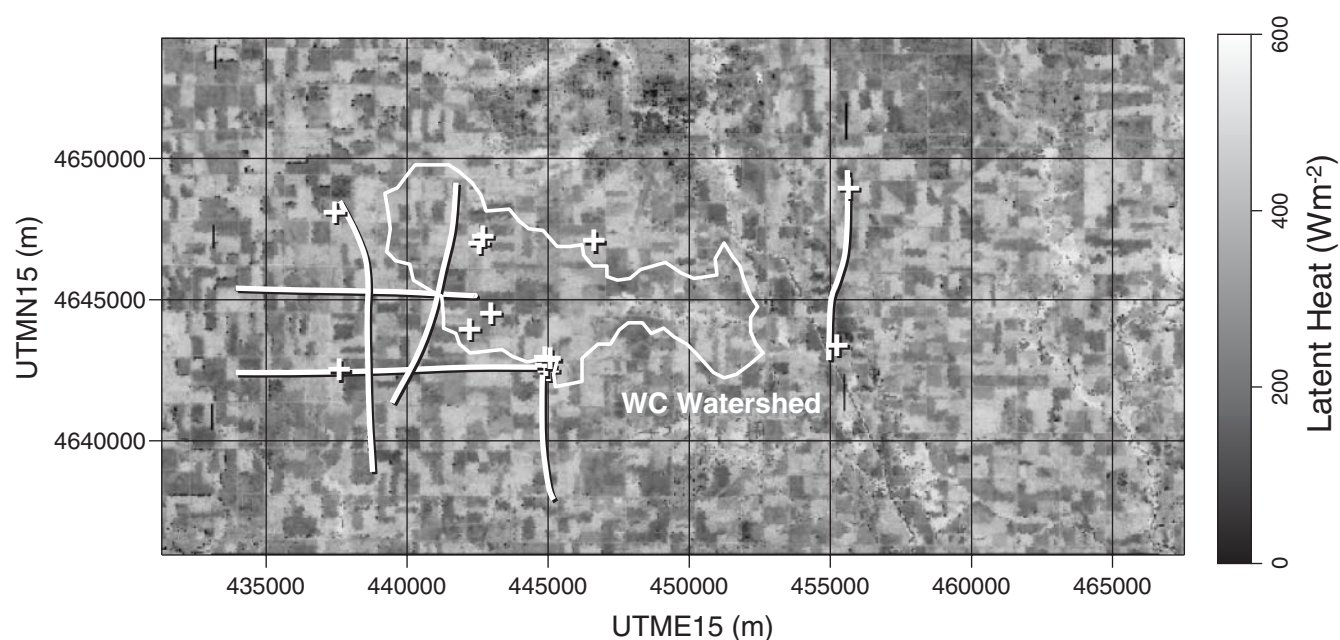


Fig. 4. Disaggregated latent heating estimates (60-m resolution) on 1 July 2002 over the Walnut Creek study area during SMACEX, projected to UTM Zone 15 coordinates. Crosses indicate locations of 12 flux towers, while the white lines demarcate the Walnut Creek Twin Otter aircraft transects. Black lines represent the scale of the 5-km ALEXI grid. The towers were located in approximately eight ALEXI grid cells.

was located within the surrounding 5-km ALEXI pixel. This makes direct comparison between tower measurements and coarse-scale flux estimates from a regional model like ALEXI highly susceptible to noise due to local scene heterogeneity, potentially masking the intrinsic accuracy of the model performance.

This effect of subpixel heterogeneity is evident in a comparison of flux measurements made at individual towers with the ALEXI estimate for the 5-km model grid cell containing the tower site (Fig. 5). The comparison between OASIS flux measurements (30-min averages at 5.5 h past sunrise, with closure correction applied) and instantaneous ALEXI estimates shows a relatively large root mean square difference (RMSD) of 64 W m^{-2} . For SGP97, a similar scatter (62 W m^{-2}) is obtained if fluxes from individual towers (hourly averages) are compared with the model predictions, as shown in Fig. 5. In this case, the four towers were located within one ALEXI grid cell. The agreement with four-tower-average fluxes (not shown) is improved (RMSD = 31 W m^{-2}), but only because the tower locations were approximately representative of the overall distribution in local land-cover conditions. Excluding the bare field site (demarcated in Fig. 5) from the average, for example, increases the RMSD to 50 W m^{-2} . In SMACEX, the high-density network of towers was equally divided between corn and soybean fields, reflecting cropping proportions determined through spectral classification (Doraiswamy et al., 2004). In this case, comparison of individual closed tower fluxes (30-min averages) with ALEXI fluxes yields an RMSD of 49 W m^{-2} , but improves to 25 W m^{-2} when both modeled and measured fluxes are averaged across the full modeling domain shown in Fig. 4.

Disaggregated fluxes are also shown in Fig. 5 in comparison with flux measurements from individual towers. The DisALEXI fluxes shown here have been re-

gregated using an analytical source weighting function (Schuepp et al., 1990) corrected for stability as described by Kustas et al. (2006). These plots demonstrate the power of disaggregation as a validation tool (compare the ALEXI and DisALEXI results). In the OASIS experiment, we get a much better idea of intrinsic model accuracy (RMSD = 35 W m^{-2}) by disaggregating down to a scale resolving both the tower footprint and the dominant length scale of heterogeneity in the landscape surrounding the tower. Similar improvement is noted for the SGP97 and SMACEX experiments, where disaggregation yields RMSD values of 38 and 28 W m^{-2} , respectively. A further benefit of disaggregation is that it can accommodate nonrepresentative measurement sites, which may provide biased estimates of the true kilometer-scale fluxes.

Tower-based EC systems provide good information about rapidly changing land-surface conditions. Note, for example, the rapidly decreasing latent heating observed at the bare soil site in SGP97 (demarcated in Fig. 5) during the 4-d dry-down period encompassed by this study. This behavior is reproduced well by the DisALEXI model, which properly interpreted the increasing surface temperature signature in the context of the low LAI in this field. The pasture sites show more constant levels of ET, as would be expected given that vegetation provides access to moisture in the root zone of the soil profile. From a model validation standpoint, flux towers provide high-resolution, time-continuous data, but only at discrete points in the modeling domain.

MODEL COMPARISONS WITH AIRCRAFT FLUXES

In contrast to fixed towers, an aircraft-based flux system provides only static snapshots of surface conditions

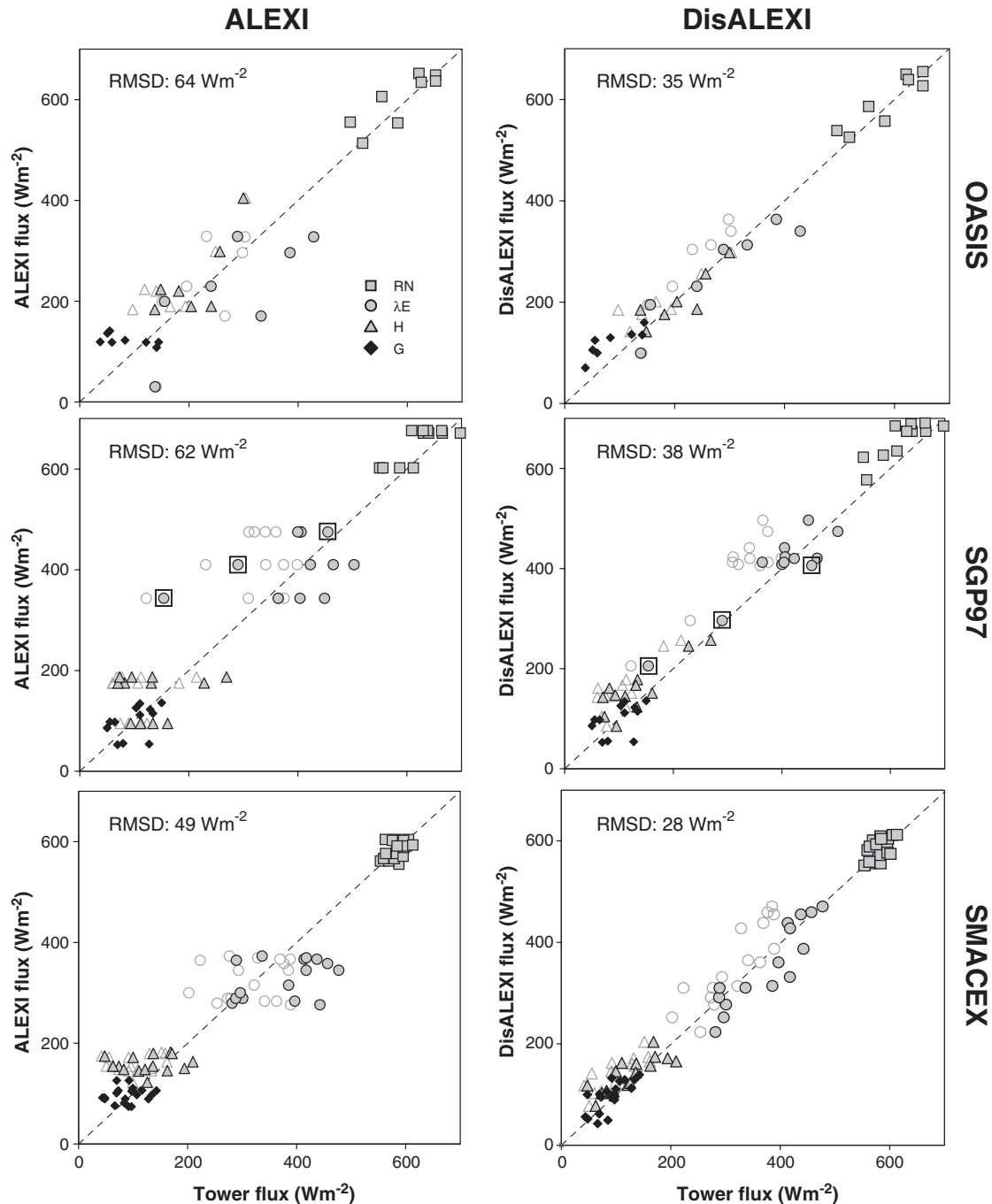


Fig. 5. Comparison of tower measurements of sensible heat (H), latent energy (λE), net radiation (RN), and soil heat flux (G) from the OASIS (30-min averages), SGP97 (hourly averages), and SMACEX (30-min averages) experiments with instantaneous flux predictions from the ALEXI and DisALEXI models (see Table 1). The ALEXI fluxes represent a 5-km average corresponding to the model grid cell containing the tower site, while the DisALEXI fluxes have been integrated across the flux tower footprint. Open H and λE symbols indicate uncorrected measurements, while gray-filled symbols represent fluxes corrected for energy budget closure by conserving the Bowen ratio. Root mean square difference (RMSD) values were computed for all four flux components combined, using closure-corrected H and λE . Latent heat fluxes associated with the bare soil site in SGP97 are highlighted with an open box.

at particular moments in time, but can sample a significantly larger area. The segmented Twin Otter latent and sensible heat flux data collected over the ER transect on 2 July 1997 during SGP97 are plotted in Fig. 6a and 7a as a function of distance along the transect. A second set of profiles demonstrates the effect of enforcing closure on average across the transect. Also plotted in

Fig. 6a and 7a are contemporaneous estimates of H and λE generated with DisALEXI, integrated across the aircraft footprint using the same analytical weighting function that was applied to the tower data (see Kustas et al., 2006, for details). This transfer function assumes that fluxes measured at the sensor height originate at some distance upwind of the transect, with the location

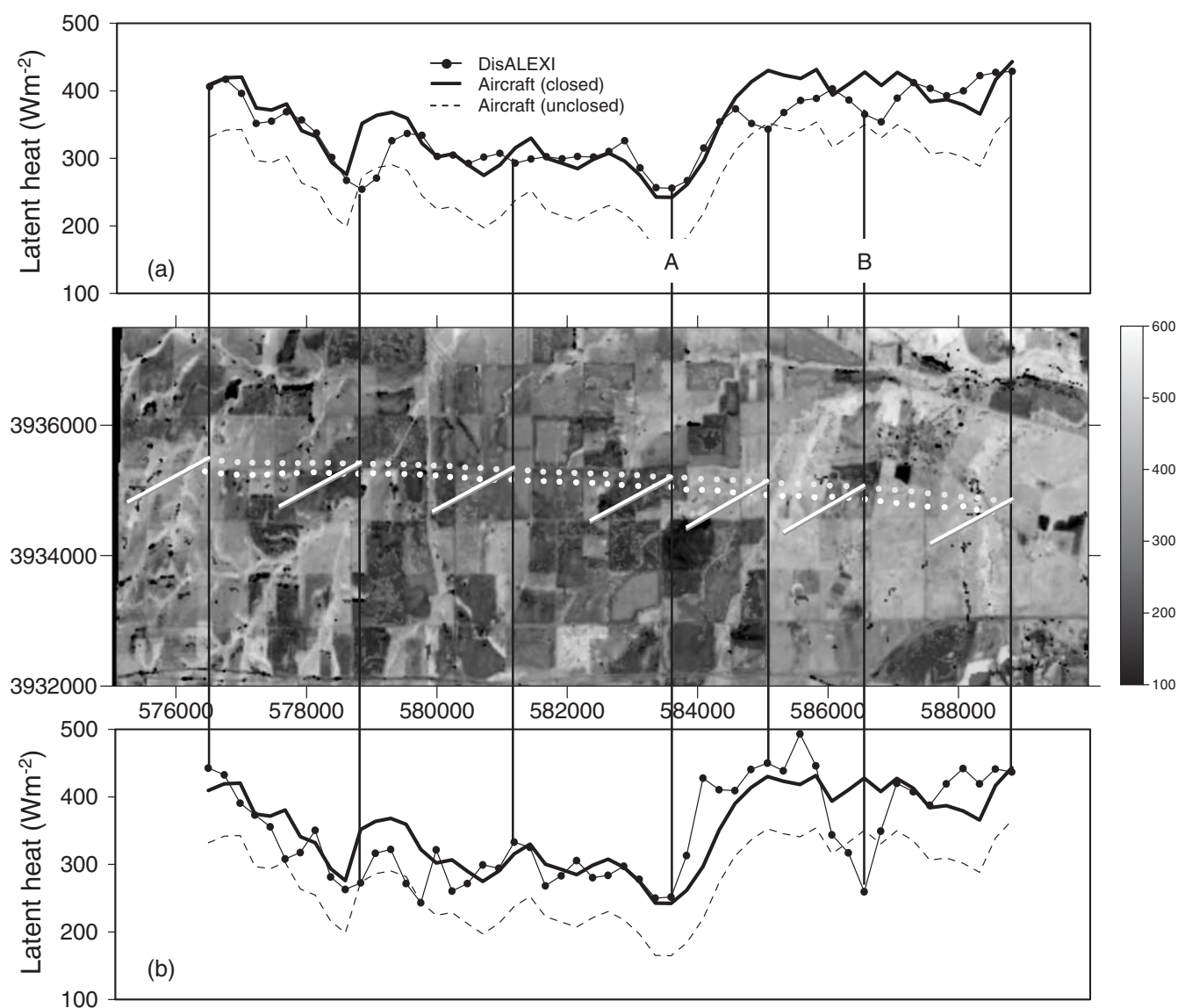


Fig. 6. Comparison of aircraft latent heat profiles acquired over the El Reno transect (SGP97) on 2 July 1997 with model predictions from DisALEXI. Uncorrected and closure-corrected aircraft fluxes as a function of position (Easting UTM, Zone 14) along transect, with DisALEXI estimates integrated (a) across the aircraft source area footprint and (b) across a swath directly beneath the aircraft. Middle panel shows DisALEXI map of latent heating with aircraft transect (upper dotted line) and maxima of footprint function (lower dotted line) indicated. White lines represent axis of footprint function (in the upwind direction).

of peak weights as demarcated on the corresponding flux maps. At the time of the TIMS image acquisition, mean winds measured at the aircraft altitude (35 m agl) were 2.7 m s^{-1} from a direction of 235 to 240°.

Using the analytical footprint function, the model reproduced the closed aircraft latent heating profile well, showing a broad decrease in evaporative flux as the aircraft moved over the area of lower vegetation cover near the center of the transect (Fig. 6a). The aircraft measurements picked up Feature A, which lagged behind the transect in accordance with prevailing wind direction. The sensible heat profile is more poorly reconstructed using this weighting function (Fig. 7a). See in particular the strong Feature B, which appears to be coincident with the overpass of a hot, dry, bare field just north of the transect. Since the wind is from the

southwest, the analytical footprint model does not capture any of the strong sensible heating from this field. An average of a swath of pixels directly underneath the transect (~300 m wide) does a better job at capturing this peak (Fig. 7b).

The fact that Feature B has no apparent counterpart signature in the aircraft λE profile suggests that the source areas for heat and water fluxes measured at height may be very different in this case, with the footprint for H peaking much closer to the aircraft transect (Kustas et al., 2006). There is mounting theoretical and observational evidence that heat and water vapor over complex terrain may be differently transported by turbulence under some conditions (e.g., Roth and Oke, 1995; McNaughton and Laubach, 1998; Asanamu and Brutsaert, 1999), particularly when the sources and sinks associated with these

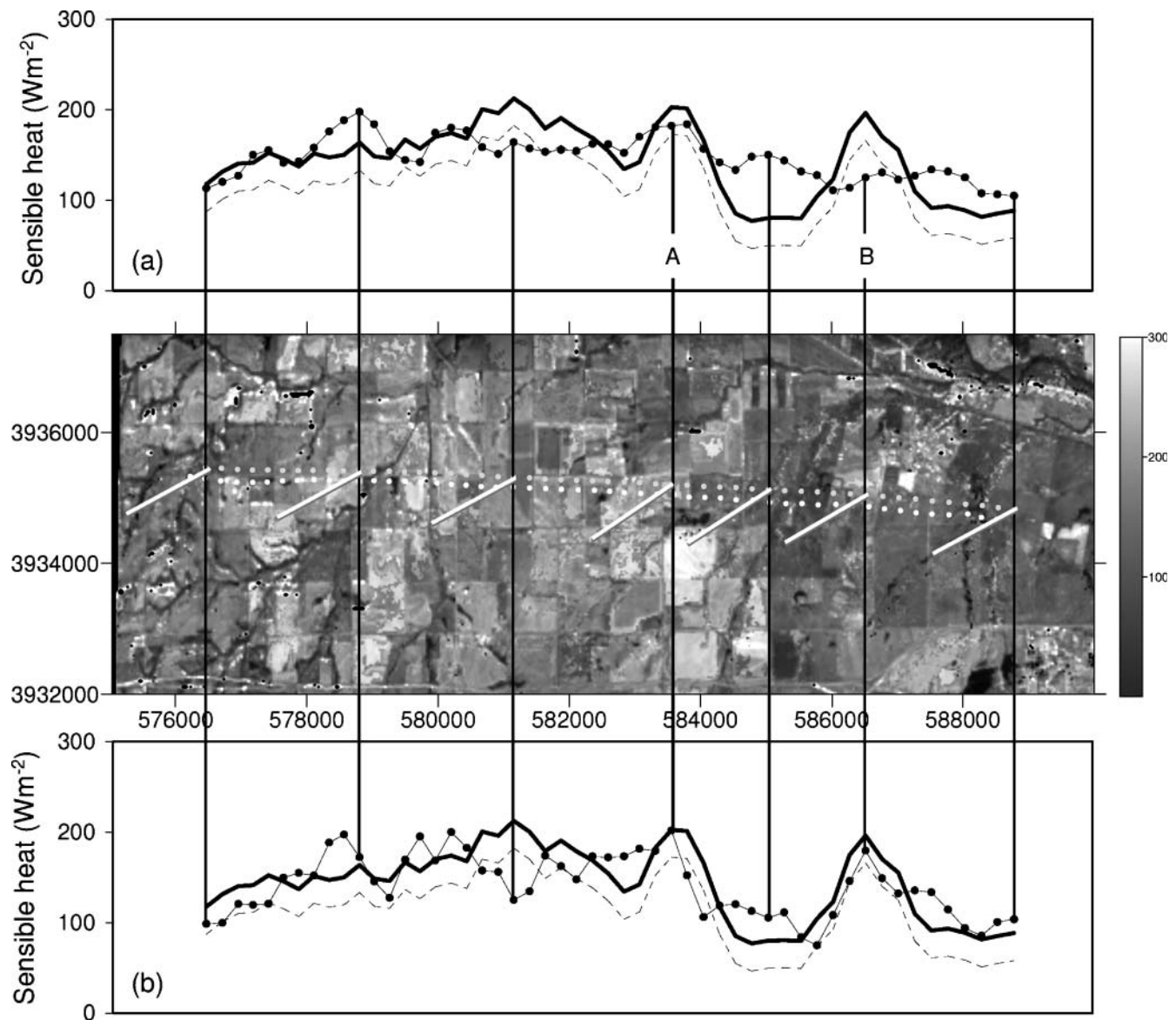


Fig. 7. Comparison of aircraft sensible heat profiles acquired over El Reno transect (SGP97) on 2 July 1997 with model predictions from DisALEXI. Uncorrected and closure-corrected aircraft fluxes as a function of position (Easting UTM, Zone 14) along transect, with DisALEXI estimates integrated (a) across the aircraft source area footprint and (b) across a swath directly beneath the aircraft. Middle panel shows DisALEXI map of latent heating with aircraft transect (upper dotted line) and maxima of footprint function (lower dotted line) indicated. White lines represent axis of footprint function (in upwind direction).

scalars are spatially separated, as in the area contributing to Feature B. The large-eddy simulation studies of Albertson and Parlange (1999), for example, showed a higher blending height for heat than for water vapor flux over a heterogeneous landscape. They suggest that these differences may be due to the fact that sensible heat is an active flux, buoyantly driving its own vertical transport and therefore constrained to smaller scales, while water vapor is more passively transported by the mean wind field and subject to horizontal mixing. The study by Kustas et al. (2006) demonstrates a novel use of high-resolution flux maps (rather than remote sensing proxies like surface temperature, land-cover class, or vegetation index) in detecting and interpreting dissimilarities in turbulent flux footprints. Ramifications for energy budget closure are discussed below.

In SMACEX, the spatial density of tower and aircraft observations was such that the two data sets compare well on average ($\text{RMSD} = 41 \text{ W m}^{-2}$ for H and λE combined) over the Walnut Creek Watershed domain, and agreement improves after closure is enforced in each data set using the average soil heat flux measured at the tower sites ($\text{RMSD} = 27 \text{ W m}^{-2}$; Anderson et al., 2005). The watershed-average Bowen ratios from each measurement system track excellently with time (Fig. 8). Both show a secular decrease as the corn and soybean canopies began to close, with a small increase from 29 June to 3 July 2002 when crops were undergoing stress from a 2-wk drought that was relieved with a rainfall event on 4 July.

Given their ability to sample large areas, aircraft are better able to quantify flux variability across a landscape than are fixed towers. Kustas et al. (2006) demonstrated

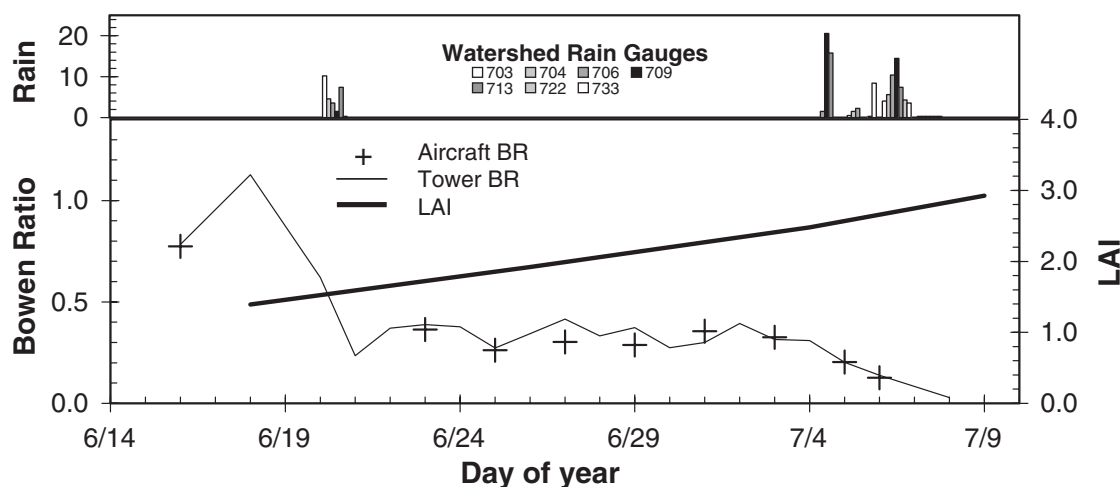


Fig. 8. Time evolution of tower and aircraft Bowen ratio (BR) measurements and MODIS leaf area index (LAI) estimates during the Soil Moisture-Atmospheric Coupling Experiment, averaged across the Walnut Creek study area. Upper panel shows daily precipitation measured at seven rain gauges in the watershed.

that the probability distribution function of fluxes across the ER study area predicted by DisALEXI was reasonably well sampled by the Twin Otter footprint, integrated along the transect. The tower footprints sampled only a fraction of the full variability contained within the scene. Combined, tower and aircraft flux data sets provide complementary information. Towers provide high-spatial-resolution, time-continuous validation at discrete points within the modeling domain, while with the aircraft data we can confirm that the model is reproducing broad spatial patterns observed at specific moments in time.

ENERGY BUDGET CLOSURE ISSUES

Other studies in this symposium addressed the question of energy budget closure in detail. In light of the aircraft findings reported above, here we briefly explore one aspect of the closure question: namely, the impact of sensor footprint on closure among EC flux measurements. Schmid (1997) noted that the nature of the relevant probability transfer function depends on whether properties are being transported turbulently or radiatively. Conductive fluxes (like the soil heat flux) will have a still different form of transfer function. And even for turbulent fluxes, the function may depend on whether the scalar in question is active or passive.

Sensors measuring net radiation and soil heat flux are generally not sampling the same source areas as the EC sensors. The former pair may be reasonably self-consistent in many cases: soil heat flux plates are typically buried in the vicinity of the tower base, while net radiometers are generally mounted on the tower with a downward-looking view. The turbulent fluxes sampled by the EC sensors, however, originate mostly upwind of the tower. In a heterogeneous landscape, this can be problematic; the land-cover conditions inside a fenced-in tower site in active grazing lands, for example, may be significantly different from those outside the fence providing the source area for H and λE .

Given these considerations, one might ask whether it is reasonable to use point-scale measurements of G to close the observed energy budget (Lloyd et al., 1997; Brotzge et al., 1999; Baldocchi, 2003). A remote-sensing model may, in fact, predict an average soil heat flux that is more representative of the source area contributing to the EC fluxes than do one or two heat-flux plate measurements made in the vicinity of the tower base. In the study with the Oklahoma Mesonet OASIS sites reported above, the EC closure errors were reduced if model estimates of soil heat flux, integrated across the turbulent flux footprint, were used to close the energy budget rather than the measured G (Anderson et al., 2004).

The question of closure assessment becomes even more complicated if, additionally, λE and H as measured by EC each have different source areas under some conditions, as discussed above. This contrast in footprint will be greatest for aircraft and tall tower systems, where the distance from source to sensor is large, and under convective conditions with lighter winds, when horizontal mixing is reduced. A set of carefully crafted aircraft transects passing over discrete sources of heat and water vapor may give us additional insight into closure errors expected due to turbulent flux footprint incompatibilities. It may be that remote-sensing models describing the two-dimensional patterns of fluxes at the land surface may be essential in assessing whether EC-derived fluxes are actually closed or not.

In comparing flux measurements with LATS model results, ambiguity in flux component source area should be weighed in selecting a closure correction technique. It may be that strict enforcement of closure among spatially incongruent measurements is unwarranted, and that relatively conservative closure schemes (across longer temporal or spatial scales) are more appropriate. For example, enforcing point-by-point closure for the segmented aircraft data shown Fig. 6 significantly alters the overall patterns of the profiles, and therefore a transect-average closure, preserving these patterns, was deemed preferable. In any case, the magnitude of the closure cor-

rection should be indicated, as the closed and unclosed fluxes may come close to bracketing reality.

CONTEXTUAL BACKGROUND THROUGH UPSCALING

Figure 9 shows an example where surface temperature and evapotranspiration are upscaled from field to continental scales, as accomplished by ALEXI and

DisALEXI using various sources of thermal remote sensing information (to maximize coverage, 14-d composites of clear-sky T_{RAD} and λE from ALEXI have been used to create the continental-scale maps). The patterns are strikingly different in each case. Because the dominant length scale of heterogeneity in the predominantly agricultural landscape of Iowa is the field scale, we see smoother patterns at much larger or smaller scales, while the watershed-scale map shows a more “checkerboard”

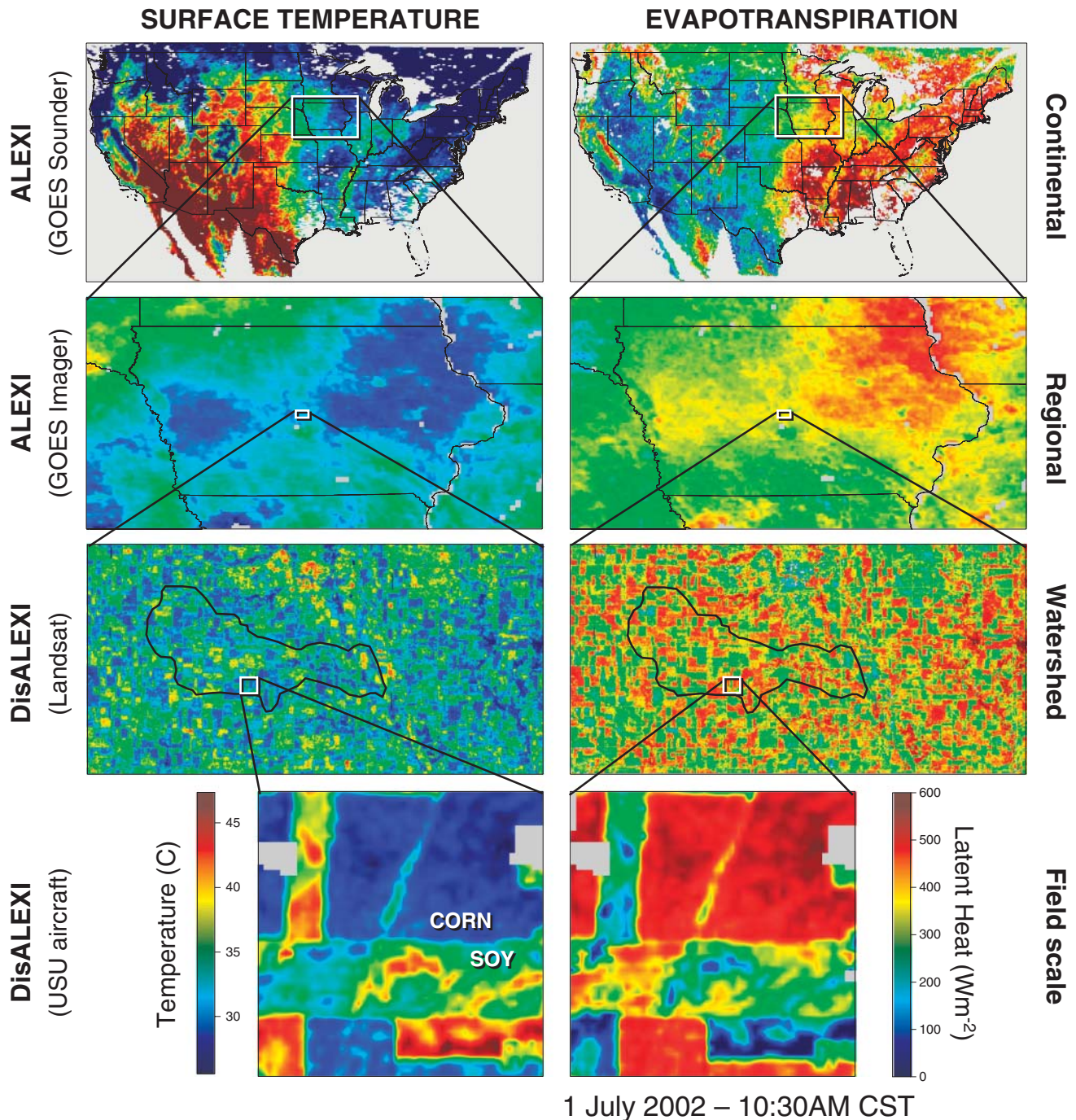


Fig. 9. Multiscale evapotranspiration (ET) maps for 1 July 2002 produced with ALEXI and DisALEXI using surface temperature data from aircraft (30-m resolution), Landsat (60 m), GOES Imager (5 km), and GOES Sounder (10 km). The continental-scale ET map is a 14-d composite of clear-sky model estimates.

distribution. Also note that the full range in variability shows up only at the field and continental scales—a narrower range exists at intermediate scales.

From a contextual standpoint, it can be very useful to be able to bracket the scale of interest (the watershed scale in the case of SMACEX). At each level, different processes influence the variability in temperature and ET. At the state scale, antecedent precipitation patterns dominate. We learn from Fig. 9 that the drought conditions experienced in the Walnut Creek Watershed on 1 July 2002 were worse than in northeastern Iowa, where it had rained only 5 d prior. At the watershed scale, the variability reflects cropping patterns—primarily corn and soybean in this case. Patchy precipitation events at the 1- to 10-km scale would have greater impact pre-emergence, when the vegetation cover is low. At the subfield scale, the effects of soil texture variations and management practices become evident. We see areas of depressed ET in the soybean field where recent weed eradication has left holes in the developing canopy, while in the corn field we see an ancient railroad bed which, though long removed, has compacted the soil and continues to impact yield and transpiration rates. The continental-scale variability reflects the strong climatic and vegetation gradients that span the USA from west to east.

UTILITY IN EXPERIMENTAL DESIGN

Primary considerations in designing a successful field experiment include site selection and instrument deployment configuration (Schmid, 1997). In the field experiments discussed above, for example, the degree to which the flux tower measurements were collectively representative of the overall experiment domain depended strongly on tower placement. An optimal sensor configuration will facilitate accurate upscaling and variability assessment with minimum redundancy. The experiment site itself must further be representative of the larger spatial and temporal extent to which the resulting findings will be applied. In both of these pre-experiment decision-making steps, a multiscale flux mapping framework like ALEXI-DisALEXI can supply valuable information based on retrospective analyses.

Long-term continental-scale flux evaluations from a daily model like ALEXI can be used to assess the climatological characteristics of various prospective experimental sites. The ALEXI model has been running operationally since 2002 on a 10-km grid covering the continental USA, using algorithms for filling data gaps due to cloud cover (Anderson et al., 2006, unpublished data). To date, three consecutive years of daily heat and water flux predictions have been archived, and modeled patterns in evaporative stress agree well with coarser resolution drought indices based on antecedent precipitation (Anderson et al., 2006, unpublished data). A climatological map of ET could serve as one layer in a geographic information system used to site a new experiment, or to flesh out an existing tower network.

In the sensor-deployment stage, high-resolution flux maps from DisALEXI can be used as a base map for evaluating sensor configuration scenarios, providing a

first guess at the expected flux distribution at the land surface under various meteorological conditions. Convolution of the disaggregated flux field with a footprint weighting function based on the observed wind statistics creates a map of fluxes as “seen” by a hypothetical EC sensor mounted in each grid cell at a prescribed height. Following Schmid and Lloyd (1999), a map of sensor location bias with respect to the field mean value can then be constructed, identifying positions where patchy surface behavior may induce unrepresentative readings for a given atmospheric state and sensor height. Alternatively, the bias associated with multiple randomly deployed sensors could be assessed through Monte Carlo simulation, prescreening the region for acceptable subdomains for tower placement in terms of topography, land use, and other logistical considerations. For long-term experiments, simulations would ideally be conducted using remote sensing from multiple seasons to capture annual variability in land-surface conditions.

These techniques can also be applied to the integrated footprint of an aircraft flying within the surface layer over complex terrain, to evaluate potential transect geometries for sampling comprehensiveness and expected flux gradients. While surrogate remotely sensed fields such as vegetation index, surface temperature, or land-use class could be used as a base map for footprint analyses (Schmid and Lloyd, 1999), their relationship with the actual surface flux distribution is indirect and can be multivalued.

CONCLUSIONS

We developed a methodology for using remote-sensing imagery to upscale tower and aircraft flux data. In this scheme, the flux measurements are used to validate a diagnostic TSEB model based primarily on surface temperature and vegetation cover inputs; then, the gridded model data provide the basis for upscaling to larger scales. The modeling system is inherently multiscale, with a regional coupled TSEB-ABL model (ALEXI) providing meteorological boundary conditions to a local model (DisALEXI) resolving the flux sensor footprint.

In comparing results from several recent field experiments, the utility of combining tower and aircraft flux data with a model-based assessment of the land-surface source and sink distribution was examined. In terms of evaluating large-scale fluxes, towers provide continuous temporal but only discrete spatial coverage across the experiment domain, while aircraft provide the complement utility. For direct comparison with regional model flux estimates across a heterogeneous landscape, a tower network must be carefully designed such that tower sites are statistically representative of the overall distribution of land-surface conditions. On the other hand, reasonable comparisons with single towers can be obtained if a flux disaggregation technique is used, breaking regional flux estimates down to the tower footprint scale. New scanning lidar techniques show potential for providing both spatially and temporally continuous water vapor flux estimates (Eichinger et al., 2006). A comparison of lidar- and DisALEXI-derived maps of latent heating

over a SMACEX study site is underway. Similar to aircraft, large-aperture scintillometers can sample sensible heat fluxes over a long baseline (e.g., Meijninger et al., 2002a, 2002b), although spatial variations along that baseline cannot be resolved.

A perennial problem in the comparison of LATS model and EC fluxes is the issue of energy budget closure. It is not clear why turbulent fluxes are consistently underestimated by EC flux systems, and if or how closure imbalance should be compensated for. Aircraft-model comparisons from SGP97 provide observational evidence of a difference in source area for turbulent fluxes of latent and sensible heating, with the sensible-heat footprint peaking closer to the nadir position of the sensor. Footprints for net radiation and soil heat flux sensors can also differ significantly in a heterogeneous landscape. Given this ambiguity, conservative methods of enforcing closure for model comparison are recommended.

In interpreting flux measurements acquired during a field experiment, considerable insight can be gained by mapping fluxes at scales both larger and smaller than the domain of the experiment. Smaller scale evaluations can be useful for understanding temporal and spatial anomalies in the flux measurement data streams, and for assessing the representativeness of the flux sensor network. Larger scale evaluations provide context for the experiment, and can be used to upscale discrete measurement sets to broader spatial and temporal scales. The multiscale ALEXI-DisALEXI modeling system was designed to perform this type of two-way scaling. In addition, the models can provide information that may be useful in designing a field experiment that will successfully meet its objectives.

ACKNOWLEDGMENTS

Funding for this research was provided by the National Aeronautics and Space Administration under grant NNG04GK89G, and in part by USDA Cooperative Agreement 58-1265-1-043.

REFERENCES

- Albertson, J.D., and M.B. Parlange. 1999. Natural integration of scalar fluxes from complex terrain. *Adv. Water Resour.* 23:239–252.
- Anderson, M.C., J.M. Norman, G.R. Diak, W.P. Kustas, and J.R. Mecikalski. 1997. A two-source time-integrated model for estimating surface fluxes using thermal infrared remote sensing. *Remote Sens. Environ.* 60:195–216.
- Anderson, M.C., J.M. Norman, W.P. Kustas, F. Li, J.H. Prueger, and J.M. Mecikalski. 2005. Effects of vegetation clumping on two-source model estimates of surface energy fluxes from an agricultural landscape during SMACEX. *J. Hydrometeorol.* 6:892–909.
- Anderson, M.C., J.M. Norman, J.R. Mecikalski, R.D. Torn, W.P. Kustas, and J.B. Basara. 2004. A multi-scale remote sensing model for disaggregating regional fluxes to micrometeorological scales. *J. Hydrometeorol.* 5:343–363.
- Asanamu, J., and W. Brutsaert. 1999. The effect of chessboard variability of the surface fluxes on the aggregated turbulence fields in a convective atmospheric surface layer. *Boundary-Layer Meteorol.* 91:37–50.
- Avissar, R., and T. Schmidt. 1998. An evaluation of the scale at which ground-surface heat flux patchiness affects the convective boundary layer using large-eddy simulations. *J. Atmos. Sci.* 55:2666–2689.
- Baldocchi, D.D. 2003. Assessing the eddy covariance technique for evaluating carbon dioxide exchange rates of ecosystems: Past, present and future. *Global Change Biol.* 9:479–492.
- Basara, J.B., and K.C. Crawford. 2002. Linear relationships between root-zone soil moisture and atmospheric processes in the planetary boundary layer. *J. Geophys. Res.* 107:1–18.
- Brotzge, J.A., and K.C. Crawford. 2003. Examination of the surface energy budget: A comparison of eddy correlation and Bowen ratio measurement systems. *J. Hydrometeorol.* 4:160–178.
- Brotzge, J.A., S. Richardson, K. Crawford, T. Horst, F. Brock, K. Humes, Z. Sorbjan, and R. Elliott. 1999. The Oklahoma Atmospheric Surface-Layer Instrumentation System (OASIS) project. p. 612–615. *In* Symp. Boundary Layers and Turbulence, 13th, Dallas, TX. 10–15 Jan. 1999. Am. Meteorol. Soc., Boston, MA.
- Brotzge, J.A., and D. Weber. 2002. Land-surface scheme validation using the Oklahoma Atmospheric Surface-Layer Instrumentation System (OASIS) and Oklahoma Mesonet data: Preliminary results. *Meteorol. Atmos. Phys.* 80:189–206.
- Campbell, G.S., and J.M. Norman. 1998. An introduction to environmental biophysics. Springer-Verlag, New York.
- Carlson, T.N. 1986. Regional-scale estimates of surface moisture availability and thermal inertia using thermal measurements. *Remote Sens. Rev.* 1:197–247.
- Choudhury, B.J., N.U. Ahmed, S.B. Idso, R.J. Reginato, and C.S.T. Daughtry. 1994. Relations between evaporation coefficients and vegetation indices studied by model simulations. *Remote Sens. Environ.* 50:1–17.
- Desjardins, R.L., J.I. MacPherson, L. Mahrt, P. Schuepp, E. Pattey, H. Neumann, D. Baldocchi, S. Wofsy, D. Fitzjarrald, H. McCaughey, and D.W. Joiner. 1997. Scaling up flux measurements for the boreal forest using aircraft-tower combinations. *J. Geophys. Res. Atmos.* 102:29125–29133.
- Diak, G.R., W.L. Bland, J.R. Mecikalski, and M.C. Anderson. 2000. Satellite-based estimates of longwave radiation for agricultural applications. *Agric. For. Meteorol.* 103:349–355.
- Doraiswamy, P.C., J.L. Hatfield, T.J. Jackson, B. Akhmedoc, J. Prueger, and A. Stern. 2004. Crop condition and yield simulations using Landsat and MODIS. *Remote Sens. Environ.* 92:548–559.
- Eichinger, W.E., D.I. Cooper, L.E. Hipps, W.P. Kustas, C.M.U. Neale, and J.H. Prueger. 2006. Spatial and temporal variation in evapotranspiration using Raman lidar. *Adv. Water Res.* 29:369–381.
- French, A.N., F. Jacob, M.C. Anderson, W.P. Kustas, W.P. Timmermans, A. Gieske, B. Su, H. Su, M.F. McCabe, F. Li, J.H. Prueger, and N. Brunzell. 2005. Surface energy fluxes with the Advanced Spaceborne Thermal Emission and Reflection radiometer (ASTER) at the Iowa 2002 SMACEX site (USA). *Remote Sens. Environ.* 99:55–65.
- Goutorbe, J.-P., T. Lebel, A. Tinga, P. Bessemoulin, J. Brouwer, A.J. Dolman et al. 1994. HAPEX-Sahel: A large scale study of land-atmosphere interactions in the semi-arid tropics. *Ann. Geophys.* 12:53–64.
- Jackson, T.J., D.M. Le Vine, A.Y. Hsu, A. Oldak, P.J. Starks, C.T. Swift, J.D. Isham, and M. Haken. 1999. Soil moisture mapping at regional scales using microwave radiometry: The Southern Great Plains hydrology experiment. *IEEE Trans. Geosci. Remote Sens.* 37:2136–2151.
- Kaharabata, S.K., P.H. Scheupp, S. Ogunjemiyo, S. Shen, M.Y. Leclerc, R.L. Desjardins, and J.I. MacPherson. 1997. Footprint considerations in BOREAS. *J. Geophys. Res.* 102:29113–29124.
- Kanemasu, E.T., S.B. Verma, E.A. Smith, L.J. Fritschen, M. Wesely, R.T. Field, W.P. Kustas, H. Weaver, J.B. Stewart, R. Gurney, G. Panin, and J.B. Moncrieff. 1992. Surface flux measurements in FIFE: An overview. *J. Geophys. Res.* 97:18547–18555.
- Koster, R., and M. Suarez. 1992. A comparative analysis of two land surface heterogeneity representations. *J. Clim.* 5:1379–1390.
- Kucharik, C.J., J.M. Norman, and S.T. Gower. 1999. Characterization of radiation regimes in nonrandom forest canopies: Theory, measurements, and a simplified modeling approach. *Tree Physiol.* 19:695–706.
- Kustas, W.P., M.C. Anderson, A.N. French, and D. Vickers. 2006. Using a remote sensing field experiment to investigate flux footprint relations and flux sampling distributions for tower and aircraft-based observations. *Adv. Water Res.* 29:355–368.
- Kustas, W.P., B.J. Choudhury, M.S. Moran, R.D. Reginato, R.D. Jackson, L.W. Gay, and H.L. Weaver. 1989. Determination of sensible heat flux over sparse canopy using thermal infrared data. *Agric. For. Meteorol.* 44:197–216.
- Kustas, W.P., G.R. Diak, and J.M. Norman. 2001. Time difference methods for monitoring regional scale heat fluxes with remote

- sensing. p. 15–29. *In* Land surface hydrology, meteorology, and climate: Observations and Modeling. AGU Water Sci. Appl. Ser. 3. Am. Geophys. Union, Washington, DC.
- Kustas, W.P., J. Hatfield, and J.H. Prueger. 2005. The Soil Moisture Atmosphere Coupling Experiment (SMACEX): Background, hydrometeorological conditions and preliminary findings. *J. Hydrometeorol.* 6:791–804.
- Kustas, W.P., and J.M. Norman. 1999. Evaluation of soil and vegetation heat flux predictions using a simple two-source model with radiometric temperatures for partial canopy cover. *Agric. For. Meteorol.* 94:13–25.
- Kustas, W.P., and J.M. Norman. 2000. A two-source energy balance approach using directional radiometric temperature observations for sparse canopy covered surfaces. *Agron. J.* 92:847–854.
- Kustas, W.P., J.M. Norman, M.C. Anderson, and A.N. French. 2003. Estimating subpixel surface temperatures and energy fluxes from the vegetation index–radiometric temperature relationship. *Remote Sens. Environ.* 85:429–440.
- Kustas, W.P., J.M. Norman, T.J. Schmugge, and M.C. Anderson. 2004. Mapping surface energy fluxes with radiometric temperature. p. 205–253. *In* D.A. Quattrochi and J.C. Luvall (ed.) Thermal remote sensing in land surface processes. CRC Press, Boca Raton, FL.
- Lloyd, C.R., P. Bessemoulin, F.D. Cropley, A.D. Culf, A.J. Dolman, J. Elbers, B. Heusikveld, J.B. Moncrieff, B. Monteny, and A. Verhoef. 1997. A comparison of surface fluxes at the HAPEX-Sahel fallow bush sites. *J. Hydrol.* 188–189:400–425.
- MacPherson, J.I. 1998. NRC Twin Otter operations in the 1997 Southern Great Plains Experiment. Lab. Tech. Rep. LTR-FR-146. Natl. Res. Council of Canada, Ottawa.
- MacPherson, J.I., and M. Wolde. 2002. NRC Twin Otter operations in the Soil Moisture–Atmosphere Coupling Experiment (SMACEX). Lab. Tech. Rep. LTR-FR-190. Natl. Res. Council of Canada, Ottawa.
- MacPherson, J.I., M. Wolde, W.P. Kustas, and J.H. Prueger. 2003. Aircraft and tower-measured fluxes over rapidly growing corn and soybean crops in central Iowa. *In* Proc. Conf. Hydrol., 17th, Long Beach, CA [CD-ROM]. 9–12 Feb. 2003. Am. Meteorol. Soc., Boston, MA.
- Mahrt, L. 1998. Flux sampling errors for aircraft and towers. *J. Atmos. Ocean. Technol.* 15:416–429.
- Mahrt, L., D. Vickers, and J. Sun. 2001. Spatial variations of surface moisture flux from aircraft data. *Adv. Water Resour.* 24:1133–1142.
- Mason, P.J. 1988. The formation of areally-averaged roughness lengths. *Q. J. R. Meteorol. Soc.* 114:399–420.
- McNaughton, K.G., and J. Laubach. 1998. Unsteadiness as a cause of non-equality of eddy diffusivities for heat and vapour at the base of an advective inversion. *Boundary-Layer Meteorol.* 88:479–504.
- McNaughton, K.G., and T.W. Spriggs. 1986. A mixed-layer model for regional evaporation. *Boundary-Layer Meteorol.* 74:262–288.
- Meijninger, W.M.L., A.E. Green, O.K. Hartogensis, W. Kohsiek, J.C.B. Hoedjes, R.M. Zuurbier, and H.A.R. De Bruin. 2002a. Determination of area-averaged water vapour fluxes with large aperture and radio wave scintillometers over a heterogeneous surface: Flevo land field experiment. *Boundary-Layer Meteorol.* 105:63–83.
- Meijninger, W.M.L., O.K. Hartogensis, W. Kohsiek, J.C.B. Hoedjes, R.M. Zuurbier, and H.A.R. De Bruin. 2002b. Determination of area-averaged sensible heat fluxes with a large aperture scintillometer over a heterogeneous surface: Flevo land field experiment. *Boundary-Layer Meteorol.* 105:37–62.
- Norman, J.M., M.C. Anderson, W.P. Kustas, A.N. French, J.R. Mecikalski, R.D. Torn, G.R. Diak, T.J. Schmugge, and B.C.W. Tanner. 2003. Remote sensing of surface energy fluxes at 10¹-m pixel resolutions. *Water Resour. Res.* 39(8):1221, doi:10.1029/2002WR001775.
- Norman, J.M., W.P. Kustas, and K.S. Humes. 1995. A two-source approach for estimating soil and vegetation energy fluxes from observations of directional radiometric surface temperature. *Agric. For. Meteorol.* 77:263–293.
- Otkin, J.A., M.C. Anderson, J.R. Mecikalski, and G.R. Diak. 2005. Validation of GOES-based insolation estimates using data from the United States Climate Reference Network. *J. Hydrometeorol.* 6:460–475.
- Palluconi, F.D., and G.R. Meeks. 1985. Thermal infrared multispectral scanner (TIMS): An investigator's guide to TIMS data. JPL Publ. 85–32. Jet Propulsion Lab., Calif. Inst. of Technol., Pasadena.
- Priestley, C.H.B., and R.J. Taylor. 1972. On the assessment of surface heat flux and evaporation using large-scale parameters. *Mon. Weather Rev.* 100:81–92.
- Prueger, J.H., J.L. Hatfield, W.P. Kustas, L.E. Hipps, J.I. MacPherson, and T.B. Parkin. 2005. Tower and aircraft eddy covariance measurements of water vapor, energy and carbon dioxide fluxes during SMACEX. *J. Hydrometeorol.* 6:954–960.
- Roth, M., and T.R. Oke. 1995. Relative efficiencies of turbulent transfer of heat, mass, and momentum over a patchy urban surface. *J. Atmos. Sci.* 52:1863–1874.
- Running, S.W., D.D. Baldocchi, D.P. Turner, S.T. Gower, P.S. Bakwin, and K.A. Hibbard. 1999. A global terrestrial monitoring network integrating tower fluxes, flask sampling, ecosystem modeling and EOS satellite data. *Remote Sens. Environ.* 70:108–127.
- Samuelson, P., and M. Tjernström. 1999. Airborne flux measurements in NOPEX: Comparison with footprint estimated surface heat fluxes. *Agric. For. Meteorol.* 98–99:205–225.
- Schmid, H.P. 1997. Experimental design for flux measurements: Matching scales of observations and fluxes. *Agric. For. Meteorol.* 87:179–200.
- Schmid, H.P. 2002. Footprint modeling for vegetation atmosphere exchange studies: A review and perspective. *Agric. For. Meteorol.* 113:159–183.
- Schmid, H.P., and C.R. Lloyd. 1999. Spatial representativeness and the location bias of flux footprints over inhomogeneous areas. *Agric. For. Meteorol.* 93:195–209.
- Schuepp, P.H., M.Y. Leclerc, J.I. MacPherson, and R.L. Desjardins. 1990. Footprint prediction of scalar fluxes from analytical solutions of the diffusion equation. *Boundary-Layer Meteorol.* 50:355–373.
- Sellers, P.J., F.G. Hall, R.D. Kelly, A. Black, D. Baldocchi, J. Berry et al. 1997. BOREAS in 1997: Experiment overview, scientific results, and future directions. *J. Geophys. Res.* 102:28731–28769.
- Song, J., and M.L. Wesely. 2003. On comparison of modeled surface flux variations to aircraft observations. *Agric. For. Meteorol.* 117: 159–171.
- Stannard, D.K., J.H. Blanford, W.P. Kustas, W.D. Nichols, S.A. Amer, T.J. Schmugge, and M.A. Weltz. 1994. Interpretation of surface flux measurements in heterogeneous terrain during the Monsoon '90 experiment. *Water Resour. Res.* 30:1227–1239.
- Stephens, B.B., S.C. Wofsy, R.F. Keeling, P.P. Tans, and M.J. Potosnak. 2000. The CO₂ Budget and Rectification Airborne Study: Strategies for measuring rectifiers and regional fluxes. p. 311–324. *In* P. Kasibhatla et al. (ed.) Inverse methods in global biogeochemical cycles. Am. Geophys. Union, Washington, DC.
- Stewart, J.B., W.P. Kustas, K.S. Humes, W.D. Nichols, M.S. Moran, and A.A.R. DeBruin. 1994. Sensible heat flux–radiometric surface temperature relationship for eight semiarid areas. *J. Appl. Meteorol.* 33:1110–1117.
- Tanner, C.B., and W.A. Jury. 1976. Estimating evaporation and transpiration from a row crop during incomplete cover. *Agron. J.* 68:239–242.
- Twine, T.E., W.P. Kustas, J.M. Norman, D.R. Cook, P.R. Houser, T.P. Meyers, J.H. Prueger, P.J. Starks, and M.L. Wesely. 2000. Correcting eddy-covariance flux underestimates over a grassland. *Agric. For. Meteorol.* 103:279–300.
- Verhoef, A., H.A.R. De Bruin, and B.J.J.M. van den Hurk. 1997. Some practical notes on the parameter kB^{-1} for sparse vegetation. *J. Appl. Meteorol.* 36:560–572.
- Vining, R.C., and B.L. Blad. 1992. Estimation of sensible heat flux from remotely sensed canopy temperatures. *J. Geophys. Res.* 97: 18951–18954.
- Wieringa, J. 1976. An objective exposure correction method for average wind speeds measured at a sheltered location. *Q. J. R. Meteorol. Soc.* 102:241–253.
- Wieringa, J. 1986. Roughness-dependent geographical interpolation of surface wind speed averages. *Q. J. R. Meteorol. Soc.* 112:867–889.
- Wilson, K., A. Goldstein, E. Falge, M. Aubinet, D. Baldocchi, P. Berbigier et al. 2002. Energy balance closure at FLUXNET sites. *Agric. For. Meteorol.* 113:223–243.
- Zhan, X., W.P. Kustas, and K.S. Humes. 1996. An intercomparison study on models of sensible heat flux over partial canopy surfaces with remotely sensed surface temperatures. *Remote Sens. Environ.* 58:242–256.